A high temperature dual-mode quartz crystal microbalance technique for erosion and thermal desorption spectroscopy measurements

Reinhard Stadlmayr,[1, a)] Paul Stefan Szabo,[1] Herbert Biber,[1] Hans Rudolf Koslowski,[2] Elisabeth Kadletz,[1] Christian Cupak,[1] Richard Arthur Wilhelm,[1] Michael Schmid,[1] Christian Linsmeier,[2] and Friedrich Aumayr[1, a)]

1) *TU Wien, Institute of Applied Physics, Fusion@ÖAW, 1040 Vienna, Austria*

2) *Forschungszentrum Jülich GmbH, Institut für Energie- und Klimaforschung - Plasmaphysik, 52425, Jülich, Germany*

(Dated: 15 November 2020)

An improved quartz crystal microbalance measurement method is described, which allows to determine erosion, implantation and release rates of thin films, during changing temperatures and up to 700 K. A quasi-simultaneous excitation of two eigenmodes of the quartz resonator is able to compensate for frequency drifts due to temperature changes. The necessary electronics, the controlling behaviour and the dual-mode temperature compensation are described. With this improved technique quantitative in-situ temperature-programmed desorption measurements are possible and the QCM can be used for quantification of thermal desorption spectroscopy measurements with a quadrupole mass spectrometer. This is demonstrated by a study of the retention and release behaviour of hydrogen isotopes in fusion-relevant materials. We find that more than 90% of the deuterium implanted into a thin film of beryllium is released during a subsequent temperature ramp up to 500 K.

Keywords: quartz-crystal-microbalance, dual-mode, overtone-mode, TPD, TDS, sputtering, erosion, retention, beryllium

---

[a)] Authors to whom correspondence should be addressed: stadlmayr@iap.tuwien.ac.at and aumayr@iap.tuwien.ac.at

I. INTRODUCTION

Quartz crystal microboalance (QCM) layer thickness measurements are based on microweighing by frequency measurements of oscillating crystals, covered with a thin film of a sample material. This technique has a long history and was established by Sauebrey already in 1959[1]. Based on the piezoelectric effect, a QCM allows measuring mass changes with high accuracy, since resonance frequencies can be determined very precisely[1–4]. QCMs have established themselves as a standard method and are widely used in industry to monitor and control coating processes, but also for laboratory experiments on film growth via molecular beam epitaxy (MBE)[5,6], or pulsed laser deposition (PLD)[7–9].

The technique can also detect mass losses, which allows to study in detail the ion-induced erosion and sputtering of surfaces. This is of high interest for investigating plasma-wall interaction processes in nuclear fusion[10–15], but also for studying space weathering effects[7,16]. While QCM measurements are usually performed near room temperature or at somewhat elevated temperatures, e.g., at an extremum of the frequency-vs-temperature curve of the quartz crystal[2], higher temperatures can be achieved with temperature compensation[17], usually limited by the phase transition from α to β quartz at $847\,\mathrm{K}$[18]. Further research showed that it is possible to operate quartz crystals even in the β phase, up to around $1500\,\mathrm{K}$[19], but with substantially reduced performance due to weaker piezoelectric coupling. Alternatively, the usage of gallium orthophosphate ($GaPO_4$) as quartz substitute allows operating temperatures up to $\approx 1200\,\mathrm{K}$[20].

Commercially available high-temperature QCMs usually require a constant operating temperature, which makes them unsuitable for temperature-programmed desorption (TPD) measurements, where continuous changes in operating temperatures are necessary. The objective of this work is to demonstrate the feasibility of a highly sensitive high-temperature QCM, capable of performing in-situ TPD measurements, by compensating frequency changes caused by temperature changes, using a dual-mode temperature compensation technique, as presented in a similar way in references 21–23. We have applied this technique up to temperatures of $700\,\mathrm{K}$.

II. BASICS OF THE QCM TECHNIQUE

Sauerbrey developed the fundamentals of the QCM technique. The basis is the fact that the resonance frequency of a quartz crystal depend on the mass of the material deposited on it. The relative change in the resonance frequency $\Delta f/f$ is given by the relative change of the mass $\Delta m/m$ (Ref. 1).

$$-\frac{\Delta f}{f} = \frac{\Delta m}{m} \tag{1}$$

Equation 1 holds true for film thicknesses much thinner than the quartz thickness. Typically, coated layers, with a thickness of some 100 nm, are about 3 orders of magnitude thinner than the quartz itself. Therefore, the initial mass m can be approximated with the quartz mass neglecting the contribution of the coated layer and the different elastic properties (acoustic impedances)[1,24,25].

Changes in the temperature and mechanical stress also cause changes in the resonance frequency of a quartz crystal, which need to be taken into account in order to reach a high sensitivity for mass changes. In fact, quartz sensors can also be used to measure these quantities[3,21,26,27].

Equation 1 can be extended to evaluate mass change rates, by considering the time derivative of the frequency, as can be seen in equation 2.

$$\frac{\Delta m}{\Delta t} = -\frac{m_0}{f_0}\frac{\Delta f}{\Delta t} \tag{2}$$

f_0 and m_0 represent the initial resonance frequency and the initial mass of the quartz crystal. A QCM allows in-situ measurements of mass changes, therefore this form of representation is more suitable.

In order to evaluate sputtering yields by particle irradiation, beam parameters can be included in equation 2. This is done by considering the target particle mass m_T, projectile flux density Φ and the surface area of the quartz sample A_q, by which the sputtering yield Y (removed atoms per incoming ion) can be determined according to equation 3[2,10]. In order to avoid an influence by the non-uniform radial sensitivity[3,28] of the quartz disc, it is necessary to distribute the projectile flux evenly over the active area of the quartz sample[2,10].

$$Y\,[\text{atoms/ion}] = \frac{1}{\Phi\, A_q\, m_T}\frac{m_0}{f_0}\frac{\Delta f}{\Delta t} \tag{3}$$

III. QCM ELECTRONICS

The QCM electronics used in the present work were originally developed at TU Wien and are described in detail by Hayderer et al.[2]. The setup measures the resonance frequency of a quartz crystal, which oscillates at 6 MHz, with an precision in the mHz range. When the quartz crystal temperature is stabilized at an extremum of it's frequency-vs-temperature curve, the precision is limited by the crystal resonance frequency drift of about 2 mHz/min and the noise of the electronics of about 5 mHz. This allows to detect mass changes in the order of 10 pg/cm^2/s, which is equivalent to a tungsten erosion rate of about 10^{-4} W monolayers/s, or an deuterium outgassing rate of about 3×10^{12} D /cm^2/s (Ref. 2 and 10).

Applying the QCM to sputtering, where implanted ions and radiation damage leads to large stress in the film, demands the use of stress compensated (SC-cut) quartz crystals. This quartz type has a lower sensitivity to thermal and mechanical stress, compared to the most commonly used AT-cut quartz crystals[2,3]. Our QCM uses plano-convex SC-cut quartz crystal resonator discs (14 mm diameter) with the product specification XA-3641 from the company KVG Quartz Crystal Technology GmbH. A thickness of 0.30 mm and a radius of curvature of 300 mm leads to a fundamental-mode frequency of 6 MHz.

Figure 1 shows the schematics of the QCM electronics, which are used for driving the quartz crystal at its resonance frequency. The quartz crystal is operated in series resonance, either at its fundamental mode (C1 mode) at 6 MHz or in C3 overtone mode, at around 18 MHz. The so-called phase box includes the main parts of the driving electronics and is located outside the ultra high vacuum (UHV) chamber. This part of the electronics is identical to that of reference 2. Electrical feedthroughs in combination with UHV coaxial cables (coax) connect the quartz crystal to the phase box. A sine wave is generated by using a PC-controlled function generator (Tektronix AFG2021) and is fed into the phase box. The function generator uses a 10 MHz oven-controlled crystal oscillator (OCXO) reference frequency (IQD IQOV-164-4) with a short term stability (Allan variance) of 0.01 ppb/s to ensure high precision. The electric circuit in the phase box provides a signal that depends

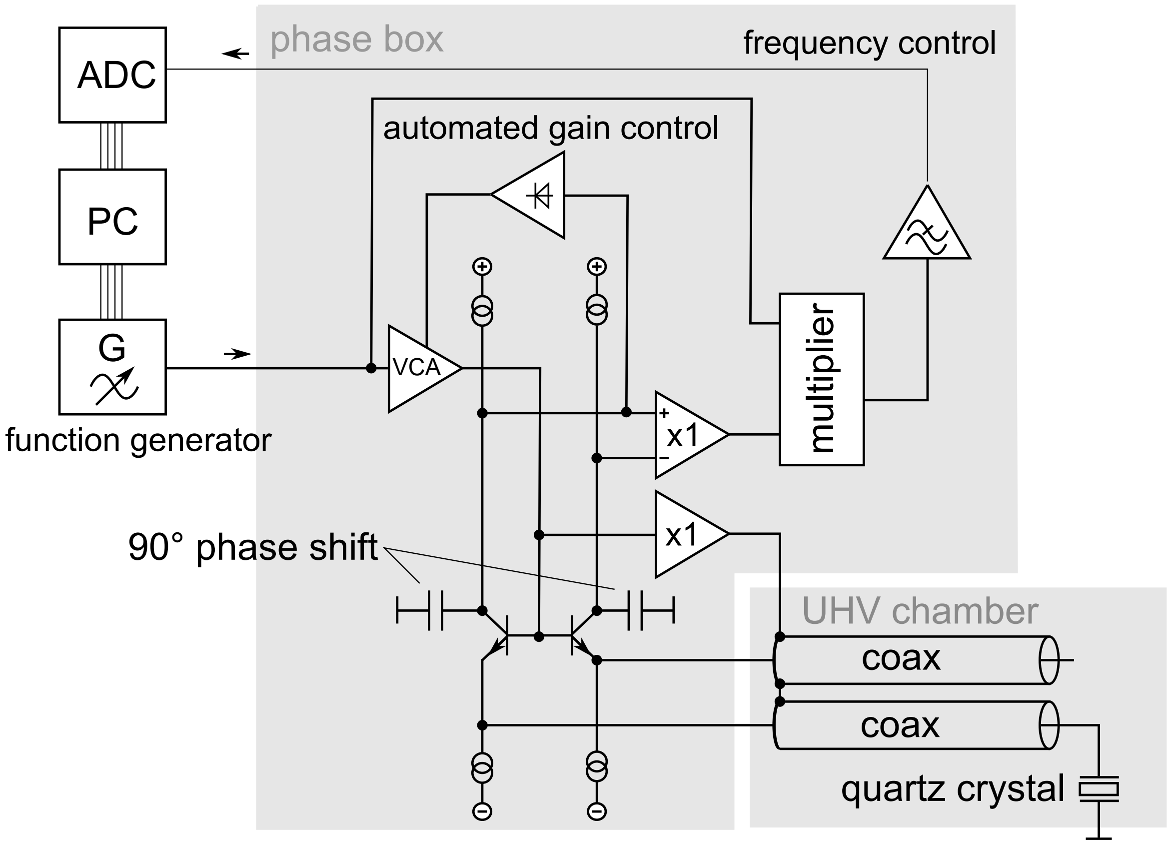

FIG. 1. QCM electronic schematics. The so-called phase box measures the phase of the admittance of the quartz crystal and provides it as an analog signal at the frequency control output. In the present setup, this output is read via an ADC, which is connected to a PC. A controlling script on this PC then adjusts the function generator output frequency to keep the quartz crystal in resonance. Adapted from ref. 2, with the permission of AIP Publishing.

on the deviation of the input frequency from the series resonance frequency of the quartz crystal, by using a phase comparison technique between current and voltage. An automated gain control with a voltage controlled amplifier (VCA) ensures a constant current through the quartz crystal. A differential setup with a separate and open ended coax cable, which has exactly the same length as the one connected to the quartz crystal, compensates for the cable capacity. At resonance, the phase shift between voltage and current is zero, which leads to a zero voltage at the frequency control output. In any other case a positive or negative voltage can be measured at the frequency control output, meaning that the actual supplied frequency is too high or too low. More details on the phase box design can be found in reference 2 (circuit diagram and component list of the phase box are available from the authors upon request). The frequency control output voltage is fed into a fast analog-digital-converter (ADC) (National Instruments USB-6210), connected to a PC. A controlling script written in Python adjusts the function generator's output frequency.

Hayderer et al. used a voltage-controlled oscillator for feeding the sine wave voltage to the phase box. The actual resonance frequency was then measured by using a frequency counter[2]. This resulted in a bulky setup. By replacing both devices with one high-precision PC-controlled function generator and a compact ADC, the size of the whole QCM electronics was substantially reduced. The function generator can be set by a digital interface, making an additional frequency counter obsolete. Furthermore, the operational frequency range is not limited to 5.9 − 6.1 MHz any more, allowing for the first time operating the TU Wien QCM in overtone mode up to 20 MHz. The use of a PC as controlling device also allows to rapidly switch between resonance frequencies and enables a quasi-simultaneous operation of two or more frequency modes.

IV. DUAL-MODE TECHNIQUE

The new digitalized QCM electronic setup allows to excite any quartz crystal modes up to 20 MHz. Only the main C-modes are of interest, because for SC-cut crystals they are insensitive to radial stress. Furthermore, the C1 and C3 modes are well separated from the side-resonances of the A and B modes, so unwanted mode coupling does not occur[3,4]. The C1 main mode is the resonance frequency used in the conventional single-mode technique, as described in reference 2. Due to the large frequency range of the function generator, care must be taken not to excite any secondary modes of the quartz crystal, which have a different sensitivity to mass and temperature changes. Except for extremely thick films, only odd overtone modes are excitable[28], therefore the second mode of interest is the C3 mode[3,4]. The C1 and C3 modes have a linear dependence on mass changes, but a different response to changes in temperature. Measuring the frequencies of both modes makes it possible to eliminate temperature effects from the data[21].

A. Principle of Dual-Mode Controlling

The improved QCM technique quasi-simultaneously excites the fundamental mode (C1 mode) and the third overtone mode (C3 mode) of a quartz crystal sample. Every 5 seconds, a proportional-integral-derivative (PID) software controller switches the sine-wave frequency generator's output between both frequencies, where the PID controlling parameters were optimized for both modes. The time constants of the controller for the C1 and C3 modes can be found in table I (We do not provide the proportional gains since they depend on the details of the implementation, such as the gain of the phase-to-voltage conversion. The proportional gains required for the C1 and C3 modes are essentially identical). We have used a controller cycle time of $\Delta t = 50\,\mathrm{ms}$. The resonance frequency recorded is the final frequency after switching to the C1 or C3 mode and running the PID controller for 5 s.

PID controlling parameters:	C1	C3
integration time T_i	1.25 s	3 s
derivative time T_d	0.06 s	0.6 s

TABLE I. PID controlling parameters for the fundamental mode C1 and overtone mode C3.

The fundamental mode frequency can be measured up to a precision in the mHz range, while the 3rd overtone mode is limited to about 100 mHz, due to increased noise and signal damping in the electronics at this frequency.

The frequency control output of the phase box provides a signal that is in first order proportional to the deviation from the resonance frequency and allows the controller to lock onto the resonance frequency (as described in section III), but only in a small frequency range. Due to the strong response of the feedback voltage at resonance, the C1 mode can be found rather easily. Here, the phase box and the controller are able to find the precise resonance frequency over a starting frequency range of $\Delta f \approx 100\,\mathrm{kHz}$ (Ref. 2).

In contrast, it is more difficult to find the C3 mode frequency, because the resonance response is less pronounced. Compared to the C1 mode, the motional capacitance of the third overtone is reduced by a factor of 1/9 due to the overtone number and another factor of $\approx 1/3$ due to the lower active area[3,28].

Furthermore, the risk of exciting secondary modes is high[3,4,29]. The frequency range for locking to the C3 mode is smaller and only in the range of about $\Delta f \approx 20\,\mathrm{kHz}$. This means the position of the frequency of the third mode needs to be preset as well as possible before the start of the dual-mode QCM operating.

Due to the plano-convex geometry of the used quartz crystal, the C3 mode frequency is lower than three times the C1 mode frequency[30,31]. Experiments have revealed a simple rule of thumb to find this frequency position:

For the crystals used, we can estimate the frequency f_3 of the C3 mode from that of the fundamental C1 mode (f_1) as described in equation 4.

$$f_3 \approx 3f_1 - 1.6 \times 10^5\,\mathrm{Hz} \tag{4}$$

This approximation is accurate within a range of 20 kHz, which is good enough for the QCM controller to lock on the precise resonance frequency.

It should be noted that the C3 mode frequency is below three times the C1 mode frequency, which provides an upper limit for the controller and avoids exciting unwanted secondary modes as well as B-mode resonance frequencies, which lie above C-mode frequencies[4]. As soon as the two resonance frequencies f_1 and f_3 have been found, when switching between the two resonances, the controller always uses the previously determined frequency value of the given mode as starting point.

B. Dual-Mode Temperature Compensation

The resonance frequency of a quartz crystal is very sensitive to changes in temperature, which causes difficulties in separating the change in the resonance frequency due to mass change and due to temperature change. A common way is to operate the quartz crystal in its fundamental mode at an elevated temperature where its frequency exhibits a minimum (see the green curve in figure 2). Here temperature changes of a few K causes only small changes in the resonance frequency[2,10,14].

In order to perform temperature-programmed desorption (TPD) measurements with a QCM the change in resonance frequency due the temperature change needs to be taken into account. The C1 and C3 modes of a quartz crystal have a linear dependence on mass changes (as can be seen in chapter VI A), but a different response to changes in temperature.

Figure 2 shows a temperature dependence of the C1 mode (f_1) and the C3 mode (f_3) of an SC-cut quartz crystal. The C3 mode shows a saddle point at 360 K, while the C1 mode has a local minimum at 435 K. Further increasing the temperature leads to a strong increase in both resonance frequencies.

By defining a beat frequency f_b (equation 5), a nearly linear dependence of f_b on the real temperature can be seen, as proposed by Pierce et al.[21].

$$f_b = 3f_1 - f_3 \tag{5}$$

The result of a test measurement is shown in figure 3, where a Be-coated quartz crystal was heated up to 700 K and f_b evaluated. Due to its almost linear temperature dependence, f_b can be used as a quartz internal thermometer[21]. In order to perform the temperature compensation, the Sauerbrey equation (equation 1) needs to be extended to also include the

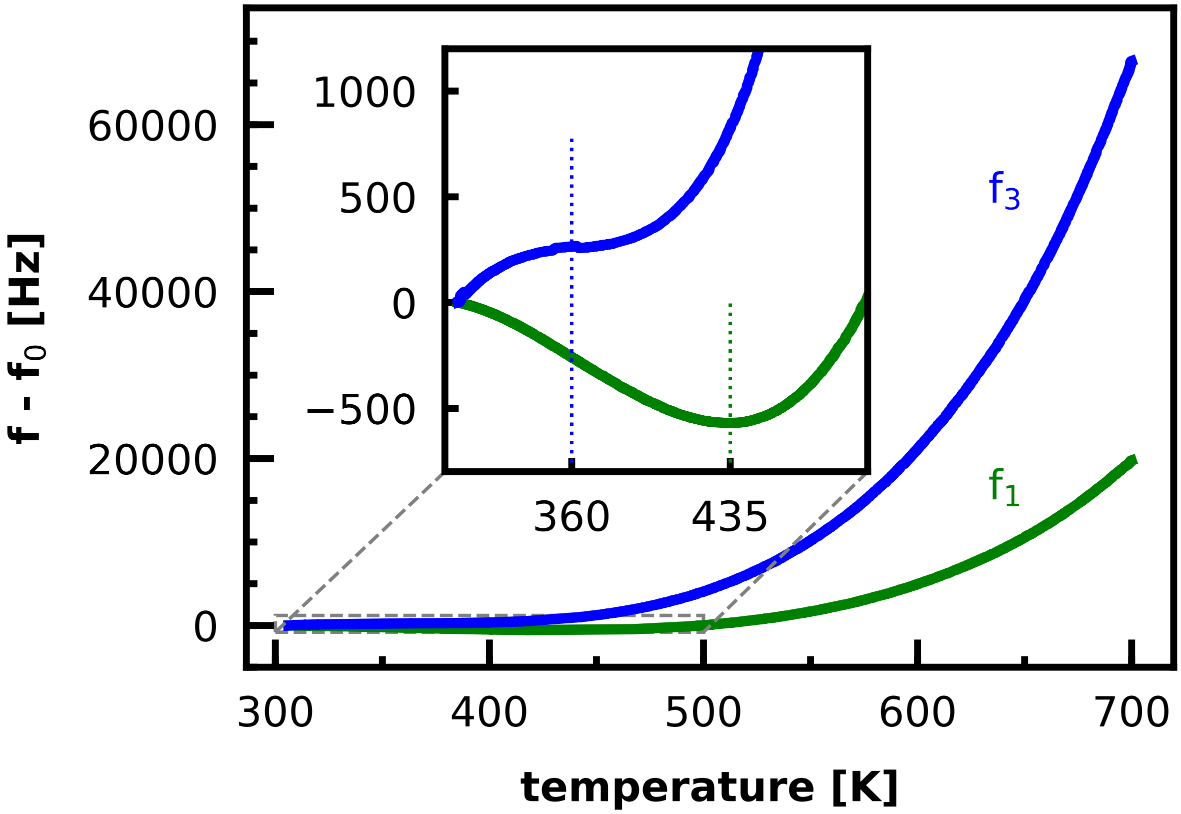

FIG. 2. (color online) Temperature responses of the C1 fundamental mode f_1 and C3 overtone mode f_3 of a Be-coated quartz crystal sample, without changes in mass. The 300 − 500 K range is enlarged in the inset.

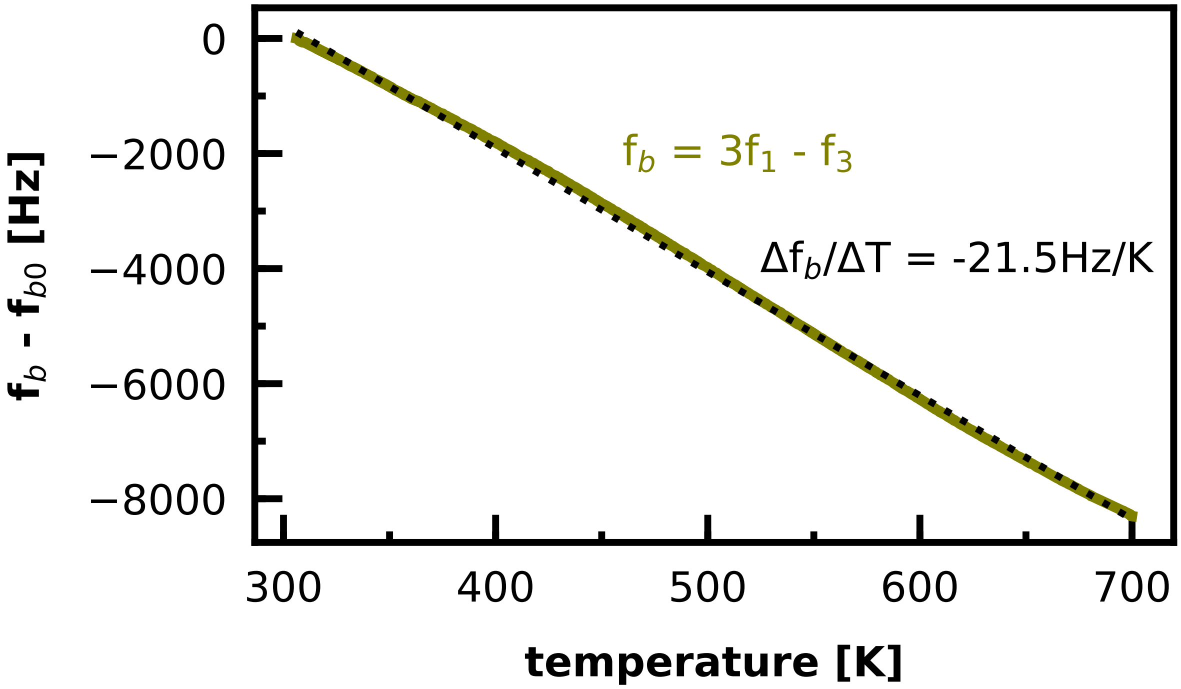

FIG. 3. (color online) The beat frequency f_b of a Be-coated quartz crystal sample, measured from room temperature to 700 K. A nearly linear behaviour can be seen. The dotted line shows a linear fit with a slope of $\Delta f_b/\Delta T = -21.5\,\mathrm{Hz/K}$.

temperature (T), as can be seen in equations 6 and 7.

$$\frac{\Delta f_1(m,T)}{f_{10}} = \frac{\Delta f_1(m)}{f_{10}} + \frac{\Delta f_1(T)}{f_{10}} = -\frac{\Delta m}{m_0} + \frac{\Delta f_1(T)}{f_{10}} \tag{6}$$

and:

$$\frac{\Delta f_3(m,T)}{f_{30}} = -\frac{\Delta m}{m_0} + \frac{\Delta f_3(T)}{f_{30}} \tag{7}$$

This extension includes both modes and the temperature dependence (index 1 for fundamental mode and index 3 for 3rd overtone mode, where '10' and '30' means initial frequency at 300 K).

Due to the nearly linear temperature dependence of the beat frequency, and as it does not depend on the mass change Δm, f_b can be used as a temperature gauge. In order to calibrate the temperature-induced frequency versus beat frequency, a frequency versus temperature measurement was conducted, without any mass change. The result is shown in figure 2. A polynomial of 5th order was used to fit this separate measurement for both eigenfrequencies, according to equations 8 and 9, as this order is sufficient for the residuals being dominated by the experimental scatter and not by the fit function.

$$f_1(T) \Rightarrow f_1(f_b) = \sum_{i=0}^{5} a_i \times (f_b)^i \tag{8}$$

$$f_3(T) \Rightarrow f_3(f_b) = \sum_{i=0}^{5} b_i \times (f_b)^i \tag{9}$$

Combining equations 6, 7, 8, 9 and conversion to mass change rate finally leads to a temperature-compensated mass change rate:

$$\begin{aligned}\frac{\Delta m}{\Delta t}\,[\text{amu/s}] = -\frac{m_0}{2}\Bigg[&\frac{1}{f_{10}}\left(\frac{\Delta f_1}{\Delta t} - \frac{\Delta f_1(f_b)}{\Delta t}\right) + \\ &\frac{1}{f_{30}}\left(\frac{\Delta f_3}{\Delta t} - \frac{\Delta f_3(f_b)}{\Delta t}\right)\Bigg]\end{aligned} \tag{10}$$

In principle, a temperature compensated mass change rate can also be realized by combining only equations 6 and 8 or only equations 7 and 9, but the numerical accuracy is increased by talking an average over both modes, as can be seen in equation 10.

Absolute temperature measurements of a quartz crystal, e.g. with a thermocouple (TC), are disadvantageous, as the temperature cannot be measured directly on the quartz crystal, but only on the sample holder. This would cause a shift between the real temperature of the quartz sample and the temperature measured via TC. The beat frequency instead is directly related to the temperature of the quartz crystal and gives a more reliable temperature information. As soon as the relation between the beat frequency and the temperature is known for the given crystal, this dual-mode technique makes measurements of the temperature with an external device obsolete during measurements of the sputtering yield or desorption. The absolute value can be obtained from calibration at room temperature, where sample holder and quartz are both at the same temperature.

V. IRRADIATION SETUP

Erosion and implantation measurements were performed under UHV conditions, with a base pressure of about 10^{-9} mbar. A sputter ion source (Speqs IQE 12/38 and Prevac IS40E1) was used to provide an ion beam with energies from $E_{kin} = 100\,\text{eV}$ to $5\,\text{keV}$ and a

D flux density of up to $\Phi \approx 10^{18}\,\mathrm{m^{-2}s^{-1}}$.

Figure 4 shows a 3D CAD drawing of the used quartz sample holder[32]. It is separated in two sections: The upper part consists of a Faraday cup with secondary electron suppression, for an accurate determination of the ion flux. The lower part includes the quartz crystal and a resistive heating system used to operate the crystal at elevated temperatures and for TPD measurements. A K-type TC, mounted laterally on the sample holder, is used for measuring the temperature.

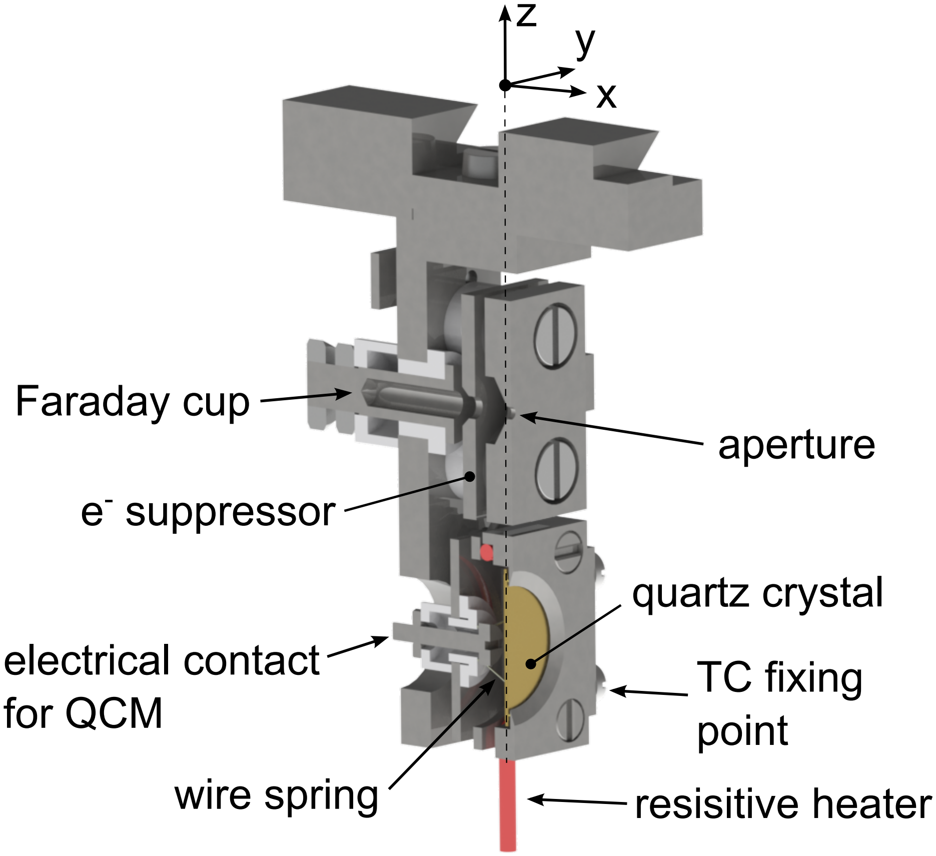

FIG. 4. (color online) Sectional drawing of the QCM sample holder. It is separated in two sections, which can be moved into the ion beam, by linear movement of the sample holder in the z-direction: At the top a Faraday cup with a secondary electron suppressor and aperture for ion beam analysis. At the bottom the quartz holder including the quartz crystal disc with a diameter of 14 mm and a resistive heater equipment. A K-type TC is mounted on one side of the holder. The dashed line indicates the rotation axis, which runs exactly through the center of the quartz crystal as well as the aperture of the Faraday cup.

A. Measurement Procedure

By using a Faraday cup, embedded in the sample holder with the quartz crystal, the ion flux Φ is measured. The beam profile is obtained by lateral displacement of the sample holder in y and z direction in mm steps. The ion beam is adjusted so that the variations of the ion current density are less than 10% over the scanning range of $5 \times 5\,\mathrm{mm}^2$. After successful adjustment of the ion beam, the quartz crystal is moved into the ion beam and the frequency change is recorded. Since no measurement of the ion beam is possible during irradiation of the sample, the ion beam flux is checked before and after every irradiation step. For sputtering yield evaluation according to equation 3, both ion flux measurements are averaged. Deviations caused by the non uniform ion beam and between both ion flux measurements are taken into account for the determination of the error bars.

VI. RESULTS

A. System Verification by Ar on Au Erosion Measurements

A measurement was carried out by irradiating an Au-coated quartz sample at room temperature to verify the expected C3 overtone mode behaviour under ion-induced erosion. The Au coating, fabricated via sputter deposition at the Institute of Solid State Physics at TU Wien, had a thickness of 500 nm. Figure 5 shows the results of this dual-mode QCM sputtering yield measurement, where an Ar^+ ion beam with an energy of $E_{kin} = 500\,\mathrm{eV}$ hits an Au-coated quartz sample under normal incidence and at room temperature (300 K). During the beam-on phase ($t = 200\,\mathrm{s} - 800\,\mathrm{s}$) a constant increase of the resonance frequency can be seen, which is equivalent to a mass loss. By evaluation the ion flux density Φ, as described in section II, the sputtering yield Y can be calculated.

Using the fundamental mode leads to a sputtering yield of $Y_{\mathrm{Ar}\rightarrow\mathrm{Au,C1}} = 2.72 \pm 0.18$ and by using the third overtone mode a sputtering yield of $Y_{\mathrm{Ar}\rightarrow\mathrm{Au,C3}} = 2.70 \pm 0.17$ can be measured. Both modes provide very similar sputtering yields, but absolute changes in the resonance frequency are three times higher while using the third overtone mode. This result confirms that Sauerbreys equation 1 holds true for the C3 overtone mode.

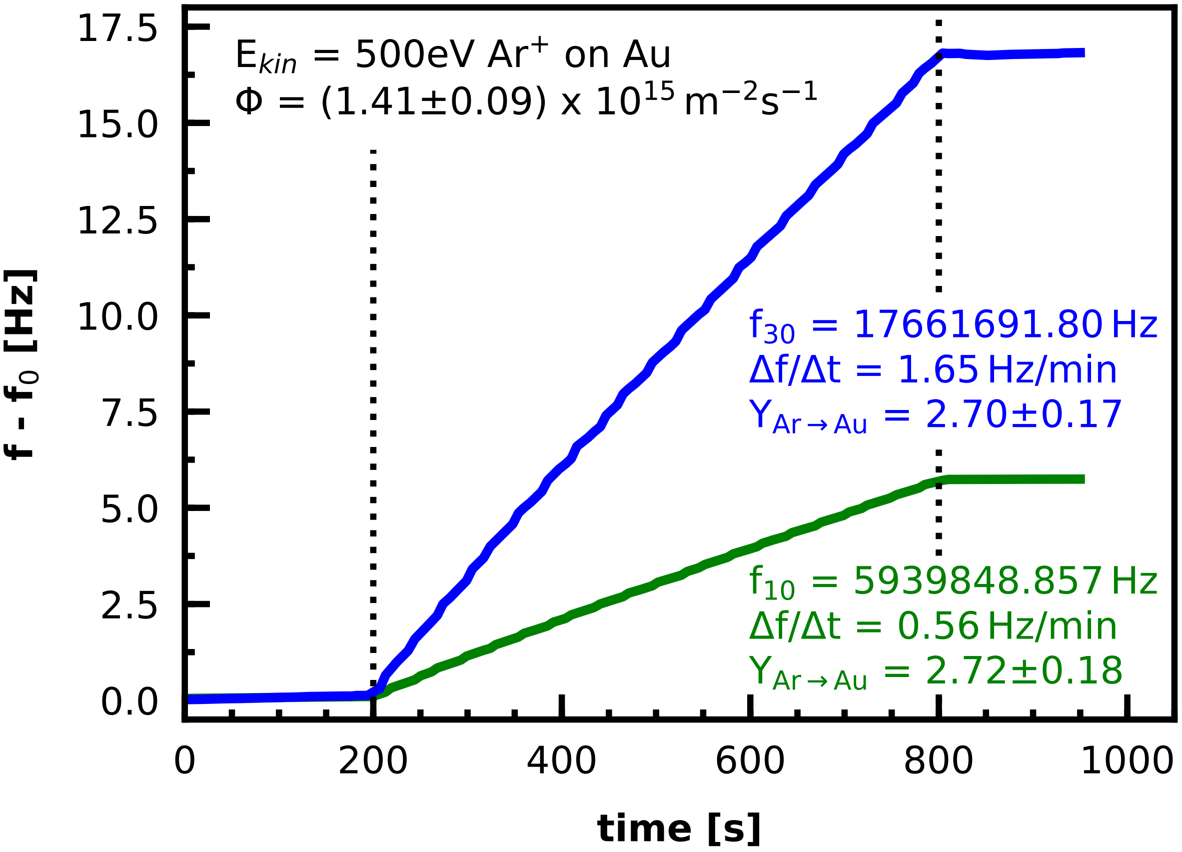

FIG. 5. (color online) Ar$^+$ on Au sputtering yield measurement, showing the QCM frequency response over time of the fundamental (C1) mode (green) and the third overtone (C3) mode (blue). During the beam-on phase between $t = 200\,\mathrm{s}$ and $t = 800\,\mathrm{s}$ an Ar$^+$ ion beam with 500 eV hits the Au-coated quartz sample under normal incidence, where a continuous increase of the resonance frequencies can be seen. The slopes $\Delta f/\Delta t$ during the beam-on phase and the ion beam flux Φ were used to evaluate the sputtering yields Y. Small wiggles in the signal are caused by the controller switching between the modes.

B. Retention and Release of D in Be

For deuterium implantation and TPD measurements, Be-coated quartz crystals were used. These coatings were fabricated by using a thermionic vacuum arc (TVA) technique at the National Institute of Laser, Plasma and Radiation Physics in Bucharest[33]. 500 nm thick Be films were deposited on top of an electrode of the quartz crystals. Before deuterium implantation, the surface was sputter-cleaned of possible oxides with an Ar ion beam at an angle of incidence of 60°.

1. *D Implantation in Be*

Implantation was performed at room temperature (300 K) and under normal incidence of the D_2^+ ions, up to a fluence of $(9.9 \pm 0.6) \times 10^{21}\,\mathrm{m}^{-2}$. Since the sputter ion source delivers the highest ion current by using D_2^+ ions, this projectile was used for implantation, where the kinetic energy of 5 keV per D_2 is equivalent to 2.5 keV per D. This factor 2 is also considered in the determination of the ion flux, where we assume that a D_2^+ ion flux corresponds to a twice as high D^+ ion flux. In our case an average D ion flux of $\Phi = (7.9 \pm 0.5) \times 10^{17}\,\mathrm{m}^{-2}\mathrm{s}^{-1}$ could be reached. At this kinetic energy of 2.5 keV per D, an implantation depth of about 70 nm can be expected, according to binary collision approximation (BCA) codes, like SRIM, or SDTrimSP[34,35]. In figure 6, the results of the implantation measurement of D in Be are shown. As the trend is very similar, only the fundamental-mode frequency f_1 is shown.

The QCM technique allows highly accurate mass change measurements, but only determination of the net mass change is possible[2]. During ion bombardment of a sample, implantation as well as sputtering and outgassing occurs. The implantation-dominated regime can be seen as a drop in the resonance frequency of the crystal, which is equivalent to a positive mass change rate and therefore an increase of the sample mass. As soon as saturation occurs, the mass change rate becomes negative, meaning that sputtering overtakes as the dominant process.

The implantation measurement shows different regions, which can be interpreted as follows (compare with figure 6):

α - Switch-on region: The frequency change is larger than what could be explained by implantation. Therefore it is dominated by thermal stress due to a slight temperature increase in the central region of the crystal, caused by the energy deposited by the ions. In the measurement, a fast frequency drop of 12 Hz can be seen and after a fluence of about $7 \times 10^{19}\,\mathrm{m}^{-2}$, the linear implantation region starts.

β - Implantation region: Here, the quartz crystal is in thermal and stress equilibrium and the implantation of projectiles continues, showing a positive and constant mass change rate of about $1.1 \times 10^{14}\,\mathrm{amu/cm^2/s}$, as well as a continuous decrease of the

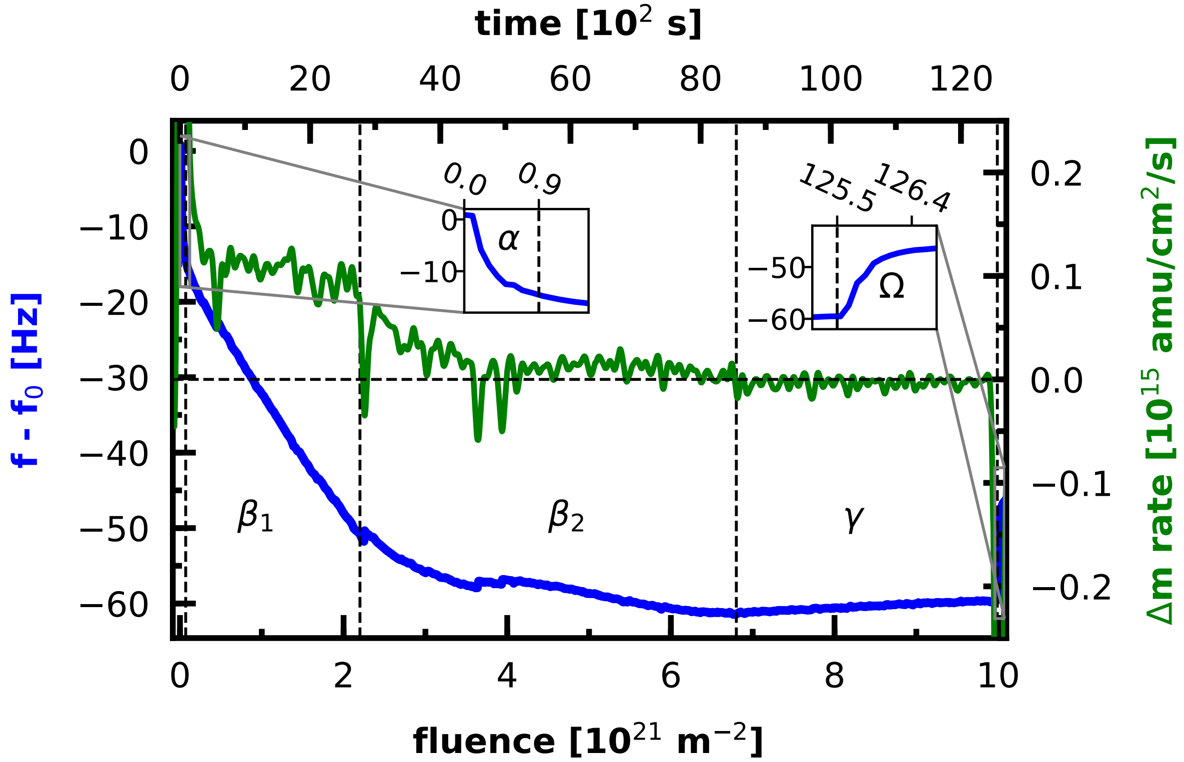

FIG. 6. (color online) Fluence dependence of the fundamental-mode resonance frequency of the quartz crystal sample (blue) and the mass change rate (Δm rate) (green) of a Be sample under D irradiation with 2.5 keV and normal incidence. Implantation of D can be seen as a decrease in the resonance frequency as well as a positive Δm rate (β_1 and β_2 region). Saturation of the sample occurs after a fluence of $6.7 \times 10^{21}\,\mathrm{m}^{-2}$, whereupon sputtering takes over as dominant process (γ region). The beam switch-on (α) and beam switch-off (Ω) regions are equivalent in height of about 12 Hz.

resonance frequency. Defects in the amorphous Be are filled up, in combination with chemical bonding to the Be as well as impurities[36], which can be seen in a high mass change rate (**$\boldsymbol{\beta_1}$ region**). After a fluence of about $2.2 \times 10^{21}\,\mathrm{m}^{-2}$ the mass change rate decreases, showing that easily accessible defects in the sample are nearly filled up (**$\boldsymbol{\beta_2}$ region**).

$\boldsymbol{\gamma}$ - Sputtering region: After a fluence of $6.7 \times 10^{21}\,\mathrm{m}^{-2}$ the sample is saturated and the mass change rate (Δm rate) becomes slightly negative, which means that sputtering overtakes as the dominant process. By evaluating the slope of the frequency response in this region, a sputtering yield of $Y_{\mathrm{D}\rightarrow\mathrm{Be}} = 0.005\,\mathrm{Be/D}$ can be obtained.

Ω - Switch-off region: After a fluence of $9.9 \times 10^{21}\,\mathrm{m}^{-2}$, the ion beam is switched off. The frequency change is due the release of the thermal stress on the quartz crystal, as the ion beam is switched off and no energy is deposited any more, as well as, possibly, due to desorption of shallow implants diffusing to the surface. As the frequency changes in the α and Ω regions are comparable, but of opposite sign (compare the two insets in figure 6), the main contribution to these changes must be attributed to thermal stress. After switching off the ion beam, no more fluence is applied. Therefore the abscissa in the insets of figure 6 is given in time units, not fluence units.

The measured mass change rate also allows to determine the total mass change during this irradiation, by integration. Here a total mass increase of $\Delta m = 381 \times 10^{15}\,\mathrm{amu/cm}^2$ could be evaluated. As the QCM technique allows to measure the total mass change only, sputtering needs to be considered. By considering a sputtering yield of $Y_{\mathrm{D}\rightarrow\mathrm{Be}} = 0.005\,\mathrm{Be/D}$, as evaluated from the γ region, which corresponds to a loss of Be and is compensated by implantation of D, the total implanted mass raises to $\Delta m = 425 \times 10^{15}\,\mathrm{amu/cm}^2$.

In the current work as well as in reference 2 we employ SC-cut quartz crystals. The resonance frequency of this particular crystal orientation is insensitive to isotropic in-plane stress, as it occurs due to ion implantation[37,38]. This is especially important if the thickness affected by the ion beam is larger than that of material added or removed, which is the case for the measurements presented in figure 6, while its impact on deposition measurements is rather limited[9]. Since the stress sensitivity of the resonance frequency depends on the azimuthal orientation of the stress and both heat conductivity and thermal expansion of quartz are anisotropic, the SC-cut is not perfectly compensated for thermal stress caused by heating the center of the crystal (in the present case, caused by the energy deposited by the impinging ions, and the edge of the crystal kept at a lower temperature). This effect can be seen in in figure 6.

total applied fluence:	9.9×10^{21}D/m^2 = 1980×10^{15}amu/cm^2	
Δm implantation:	$+425 \times 10^{15}$amu/cm^2	21.5%
Δm TPD ($m = 4$ peak):	-394×10^{15}amu/cm^2	19.9%

TABLE II. Comparison of the total applied fluence to the measured mass change (Δm) during implantation of $\mathbf{D_2}$ **in Be** and subsequent TPD. The percentages refer to the total applied fluence. The mass loss measured with the QCM (using dual-mode temperature compensation) during TPD is lower compared to the mass increase caused by implantation.

2. TPD Measurements

After the implantation a TPD measurement was initiated. The resistive heater wires of the sample holder in combination with a computer-controlled current supply and an attached TC (compare with section V) were used to perform a heating ramp with a rate of 1.5 K/min. A quadrupole mass spectrometer (QMS) attached to the chamber, with a distance of about 10 cm of the sensor head to the sample, was used to analyse the outgassing elements and molecules.
In figure 7, the TPD results can be seen, from room temperature to 500 K. The QMS signal shows a pronounced $m/q = 4$ (D_2) peak at a temperature of 423 K, while in the $m/q = 2$ signal (H_2 and D) only a continuous decrease of the signal can be seen. The blue line in this signal shows the resulting mass change rate evaluated simultaneously via the dual-mode QCM technique. It confirms a negative mass change, peaking at 423 K and thus clearly displays the outgassing of D, which desorbs as D_2. By integrating the mass change rate over this peak, a total mass loss of $\Delta m = -394 \cdot 10^{15}$amu/cm^2 could be quantitatively evaluated.

In table II, the mass change rates evaluated during implantation and during the TPD are compared and compared to the total applied fluence. During implantation, 21.5% of the total applied D fluence was implanted into the sample, while during the TPD a value of 19.9% was emitted. Although an error in the total applied fluence of about 6% needs to be considered here, it is noteworthy that about 93% of the implanted D is released during the TPD temperature ramp up to 500 K.

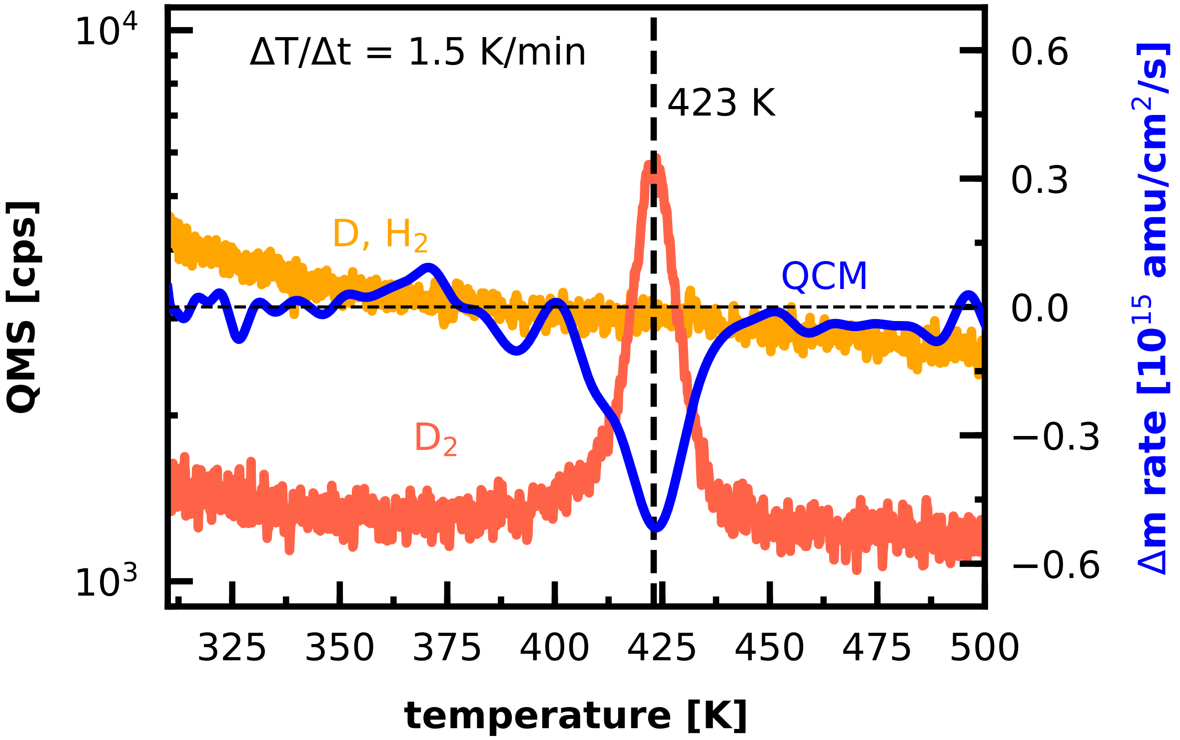

FIG. 7. (color online) TPD result after D implantation in Be. The QMS revealed a pronounced D_2 outgassing, peaking at 423 K with a QMS count rate of 6×10^3 cps. The QCM confirms this peak, showing a negative peak of the mass change rate. By integrating over this peak, a total mass loss of $\Delta m = -394 \cdot 10^{15}$amu/cm^2 can be evaluated.

VII. SUMMARY AND CONCLUSION

An improvement of the TU Wien QCM technique was presented, which allows to operate a quartz crystal sample in overtone modes. A quasi-simultaneous excitation of the fundamental mode (C1) and the third overtone mode (C3) of a quartz crystal allows to compensate for frequency changes caused by temperature changes. This principle is based on an idea from references 21–23. We were able to show that this technique can be used to perform high-temperature QCM measurements up to 700 K.

The QCM electronics described in reference 2 were modified by using a software-controlled high-precision function generator, which extends the driving frequency range up to 20 MHz. This maximum frequency is limited by the function generator used, but could be further increased by using a different generator. However, care must be taken that the performance of the current phase-detection electronics becomes less satisfactory at high frequencies, and at the same time the admittance change of the quartz crystal at the resonance also decreases with overtone number, which makes it more difficult to lock on the resonance frequencies with higher precision. Furthermore, the broad frequency range increases the risk of exciting unwanted side-mode resonances.

The quasi-simultaneous excitation of two eigenmodes by switching between the frequencies is advantageous, as the driving electronics only has to be designed once. Furthermore, interference by simultaneous excitation of several resonances is intrinsically avoided. It was shown that erosion rates can also be evaluated with the C3 mode.

This technique was used for the first time to investigate the implantation and release behaviour of D in Be. A total D fluence of $9.9 \times 10^{21}\,\mathrm{m}^{-2}$ was applied, where the QCM mass change measurements during implantation showed that 21.5% of the applied D fluence was implanted. A subsequent TPD measurement in combination with the new QCM dual-mode temperature compensation technique revealed a total mass release of 20% of the total applied D fluence. This means that over 90% of the implanted D is again released during the temperature scan up to 500 K, with a pronounced release peak of D observed very clearly at a temperature of 423 K.

Oberkofler et al.[39] found out that a threshold fluence needs to be implanted first in order to see this 'low-temperature' release peak at all, whereon the maximum of this peak shifts to lower temperatures at higher fluences. Furthermore he found out that between 700 K and 850 K further D is released. This was also confirmed by Eichler et al.[40].

Since in a future fusion facility, such as ITER, temperatures around 900 K are expected for a Be blanket plasma-facing-component, the fusion fuel implanted in the wall will immediately outgas and therefore the retention will be low[41–44].

Unfortunately, this temperature range is not accessible with our current QCM technique. As mentioned above, beyond 846 K the stable phase of quartz is the β phase, and on returning to the α phase at lower temperatures would make the quartz crystals essentially unusable due to twinning. Even if the β phase is piezoelectric, its low coupling constant would make excitation of the 3rd harmonic overtone very difficult. Furthermore, it is unclear whether this particular crystal orientation is still stress-compensated in the β phase. A better alternative for high-temperature measurements would be the use of gallium orthophosphate ($GaPO_4$)

crystals, which are stable up to 1200 K and also provide stronger piezoelectric coupling than SiO_2[20].

ACKNOWLEDGMENTS

The authors are grateful to C.P. Lungu at the National Institute for Laser, Plasma, and Radiation Physics in Bucharest for the preparation of Be samples and to C. Eisenmenger-Sittner at the Institute of Solid State Physics at TU Wien for the preparation of Au samples. This work has been carried out within the framework of the EUROfusion Consortium and has received funding from the Euratom research and training programme 2014-2018 and 2019-2020 under grant agreement No 633053. The views and opinions expressed herein do not necessarily reflect those of the European Commission.
Financial support has also been provided by KKKÖ (commission for the coordination of fusion research in Austria at the Austrian Academy of Sciences - ÖAW) and by the Austrian Science Fund FWF (Project No. I 4101-N36).

DATA AVAILABILITY

The data that support the findings of this study are available from the corresponding author upon reasonable request.

REFERENCES

[1] G. Sauerbrey, Zeitschrift für Physik **155**, 206 (1959).

[2] G. Hayderer, M. Schmid, P. Varga, H. P. Winter, and F. Aumayr, Review of Scientific Instruments **70**, 3696 (1999).

[3] E. Benes, M. Gröschl, W. Burger, and M. Schmid, Sensors and Actuators A: Physical **48**, 1 (1995).

[4] M. Schmid, *Möglichkeiten und Grenzen der Schwingquarz-Schichtdickenmessung*, PhD thesis, TU Wien (1989).

[5] D. S. Katzer, N. Nepal, D. J. Meyer, B. P. Downey, V. D. Wheeler, D. F. Storm, and M. T. Hardy, Applied Physics Express **8**, 085501 (2015).

[6] C. D. Theis and D. G. Schlom, Journal of Crystal Growth **174**, 473 (1997).

[7] P. S. Szabo, R. Chiba, H. Biber, R. Stadlmayr, B. M. Berger, D. Mayer, A. Mutzke, M. Doppler, M. Sauer, J. Appenroth, J. Fleig, A. Foelske-Schmitz, H. Hutter, K. Mezger, H. Lammer, A. Galli, P. Wurz, and F. Aumayr, Icarus **314**, 98 (2018).

[8] A. A. Voevodin and S. J. P. Laube, Surface and Coatings Technology **76-77**, 670 (1995).

[9] G. Franceschi, M. Schmid, U. Diebold, and M. Riva, Rev Sci Instrum **91**, 065003 (2020).

[10] A. Golczewski, K. Dobes, G. Wachter, M. Schmid, and F. Aumayr, Nuclear Instruments and Methods in Physics Research Section B: Beam Interactions with Materials and Atoms **267**, 695 (2009).

[11] R. Stadlmayr, P. S. Szabo, B. M. Berger, C. Cupak, R. Chiba, D. Blöch, D. Mayer, B. Stechauner, M. Sauer, A. Foelske-Schmitz, M. Oberkofler, T. Schwarz-Selinger, A. Mutzke, and F. Aumayr, Nuclear Instruments and Methods in Physics Research Section B: Beam Interactions with Materials and Atoms **430**, 42 (2018).

[12] R. Stadlmayr, P. S. Szabo, D. Mayer, C. Cupak, T. Dittmar, L. Bischoff, S. Möller, M. Rasiński, R. A. Wilhelm, W. Möller, and F. Aumayr, Journal of Nuclear Materials **532** (2020).

[13] R. Stadlmayr, P. S. Szabo, D. Mayer, C. Cupak, W. Möller, and F. Aumayr, Physica Scripta **T171** (2020).

[14] B. M. Berger, R. Stadlmayr, D. Blöch, E. Gruber, K. Sugiyama, T. Schwarz-Selinger, and F. Aumayr, Nuclear Materials and Energy **12**, 468 (2017).

[15] K. Dobes, M. Köppen, M. Oberkofler, C. P. Lungu, C. Porosnicu, T. Höschen, G. Meisl, C. Linsmeier, and F. Aumayr, Nuclear Instruments and Methods in Physics Research Section B: Beam Interactions with Materials and Atoms **340**, 34 (2014).

[16] P. S. Szabo, H. Biber, N. Jäggi, M. Brenner, D. Weichselbaum, A. Niggas, R. Stadlmayr, D. Primetzhofer, A. Nenning, A. Mutzke, M. Sauer, J. Fleig, A. Foelske-Schmitz, K. Mezger, H. Lammer, A. Galli, P. Wurz, and F. Aumayr, The Astrophysical Journal **891**, 100 (2020).

[17] V. M. Mecea, J. O. Carlsson, P. Heszler, and M. Bârtan, Vacuum **46**, 691 (1995).

[18] R. S. Coe and M. S. Paterson, Journal of Geophysical Research (1896-1977) **74**, 4921 (1969).

[19] T. Uno, H. Tashiro, and S. Noge, IEEJ Transactions on Electronics, Information and Systems **131**, 1150 (2011).

[20] H. Thanner, P. W. Krempl, W. Wallnöfer, and P. M. Worsch, Vacuum **67**, 687 (2002).

[21] D. E. Pierce, Y. Kim, and J. R. Vig, IEEE Transactions on Ultrasonics, Ferroelectrics, and Frequency Control **45**, 1238 (1998).

[22] S. S. Schodowski, in *Proceedings of the 43rd Annual Symposium on Frequency Control* (IEEE, 1989) pp. 2–7.

[23] A. Benjaminson and S. C. Stallings, in *Proceedings of the 43rd Annual Symposium on Frequency Control* (IEEE, 1989) pp. 20–26.

[24] E. Benes, Journal of Applied Physics **56**, 608 (1984).

[25] C. Lu and O. Lewis, Journal of Applied Physics **43**, 4385 (1972).

[26] F. J. Azcondo and J. Peire, in *Proceedings IECON '91: 1991 International Conference on Industrial Electronics, Control and Instrumentation* (1991) pp. 2580–2585 vol.3.

[27] R. J. Besson, J. J. Boy, B. Glotin, Y. Jinzaki, B. Sinha, and M. Valdois, IEEE Transactions on Ultrasonics, Ferroelectrics, and Frequency Control **40**, 584 (1993).

[28] M. Schmid, E. Benes, W. Burger, and V. Kravchenko, IEEE Transactions on Ultrasonics, Ferroelectrics, and Frequency Control **38**, 199 (1991).

[29] M. Küstner, W. Eckstein, E. Hechtl, and J. Roth, Journal of Nuclear Materials **265**, 22 (1999).

[30] D. S. Stevens and H. F. Tiersten, The Journal of the Acoustical Society of America **79**, 1811 (1986).

[31] E. Benes, M. Schmid, and V. Kravchenko, The Journal of the Acoustical Society of America **90**, 700 (1991).

[32] B. M. Berger, *Laboratory work on plasma-wall-interaction processes relevant for fusion experiments*, PhD thesis, TU Wien (2017).

[33] C. P. Lungu, I. Mustata, V. Zaroschi, A. M. Lungu, A. Anghel, P. Chiru, M. Rubel, P. Coad, and G. F. Matthews, Physica Scripta **T128**, 157 (2007).

[34] J. F. Ziegler, M. D. Ziegler, and J. P. Biersack, Nuclear Instruments and Methods in Physics Research Section B: Beam Interactions with Materials and Atoms **268**, 1818 (2010).

[35] A. Mutzke, R. Schneider, W. Eckstein, R. Dohmen, K. Schmid, U. v. Toussaint, and G. Badelow, IPP Report 2019-02 (2019), 10.17617/2.3026474.

[36] K. Sugiyama, C. Porosnicu, W. Jacob, I. Jepu, and C. P. Lungu, Nuclear Materials and Energy **6**, 1 (2016).

[37] E. P. EerNisse, in *29th Annual Symposium on Frequency Control* (IEEE, 1975) pp. 1–4.

[38] E. P. EerNisse, in *30th Annual Symposium on Frequency Control* (IEEE, 1976) pp. 8–11.

[39] M. Oberkofler, M. Reinelt, A. Allouche, S. Lindig, and C. Linsmeier, Physica Scripta **T138**, 014036 (2009).

[40] M. Eichler, Nuclear Materials and Energy **19**, 440 (2019).

[41] P. Vladimirov, D. Bachurin, V. Borodin, V. Chakin, M. Ganchenkova, A. Fedorov, M. Klimenkov, I. Kupriyanov, A. Moeslang, M. Nakamichi, T. Shibayama, S. V. Til, and M. Zmitko, Fusion Science and Technology **66**, 28 (2014).

[42] M. Kikuchi, K. Lackner, and T. Minh Quang, eds., *Fusion Physics* (IAEA, International Atomic Energy Agency, 2012).

[43] G. Janeschitz, Journal of Nuclear Materials **290-293**, 1 (2001).

[44] V. Barabash, G. Federici, R. Matera, A. R. Raffray, and I. Home Teams, Physica Scripta **T81**, 74 (1999).

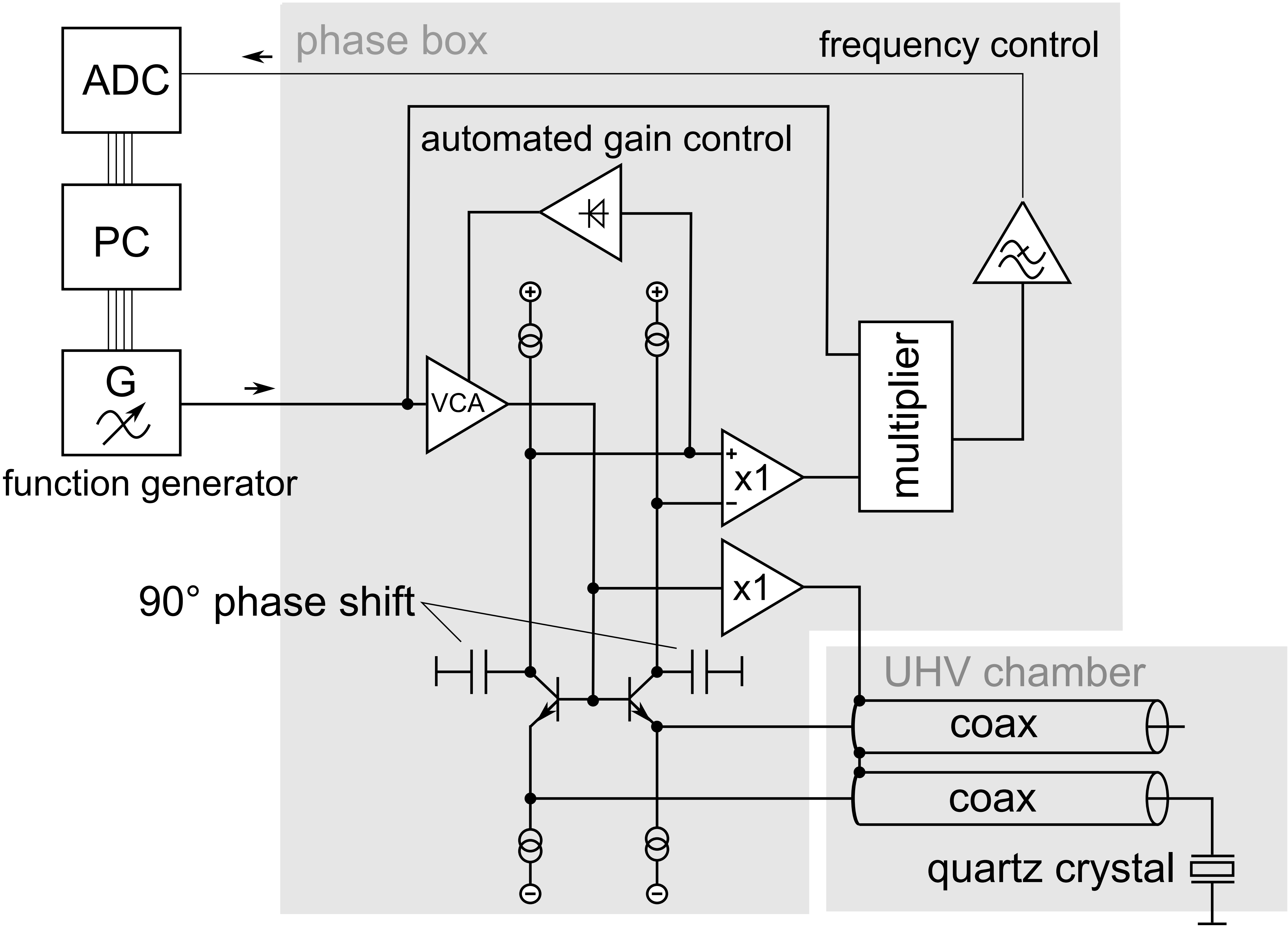
phase box
frequency control
ADC
PC
G
function generator
automated gain control
VCA
+
x1
−
x1
multiplier
90° phase shift
UHV chamber
coax
coax
quartz crystal

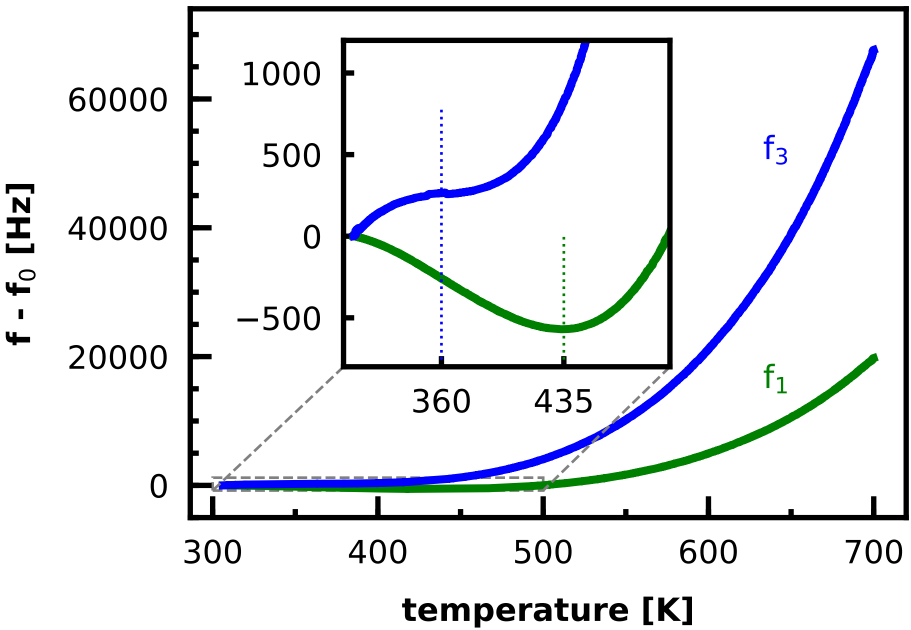

f - f_0 [Hz]
60000
40000
20000
0
300
400
500
600
700
temperature [K]
f_3
f_1
1000
500
0
−500
360
435

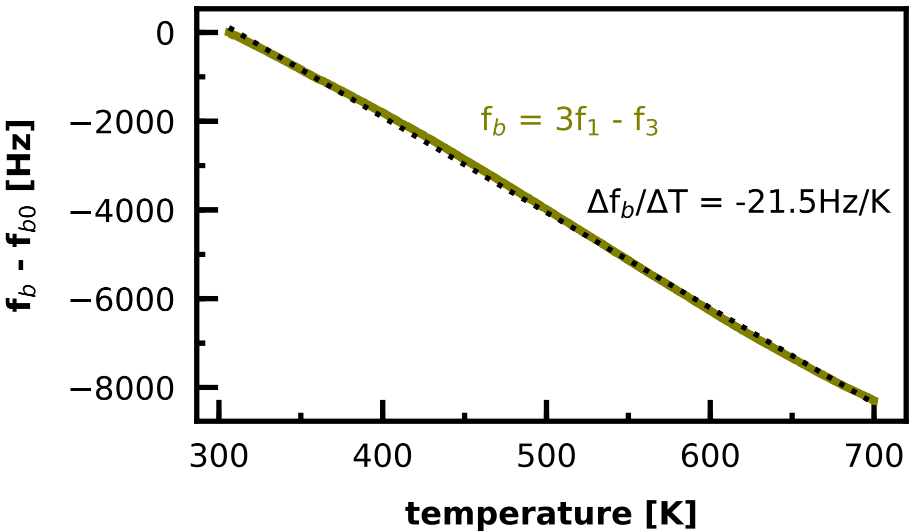
f_b - f_{b0} [Hz]
0
−2000
−4000
−6000
−8000
300
400
500
600
700
temperature [K]
$f_b = 3f_1 - f_3$
$\Delta f_b/\Delta T$ = -21.5Hz/K

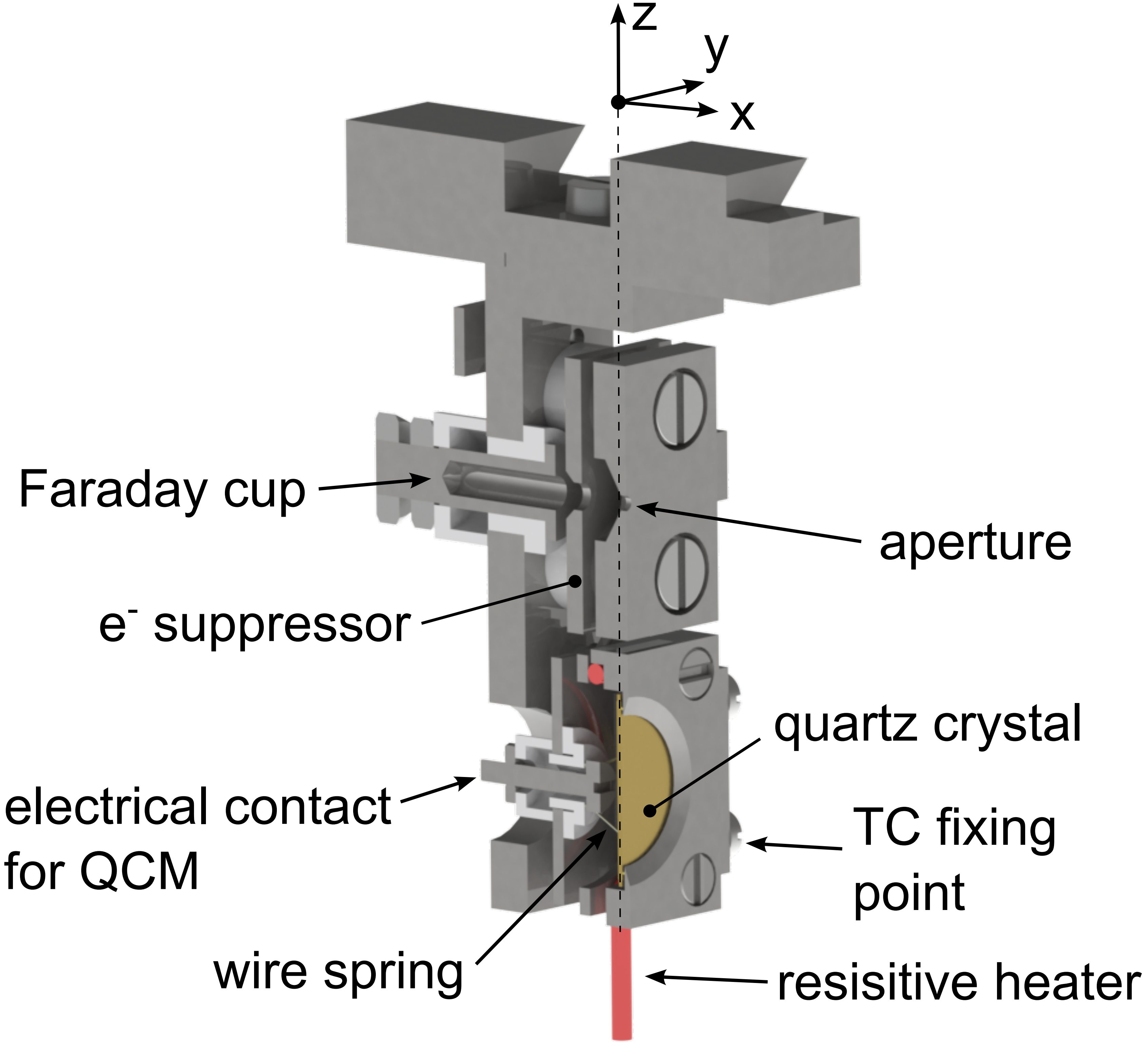
z
y
x
Faraday cup
aperture
e⁻ suppressor
quartz crystal
electrical contact for QCM
TC fixing point
wire spring
resisitive heater

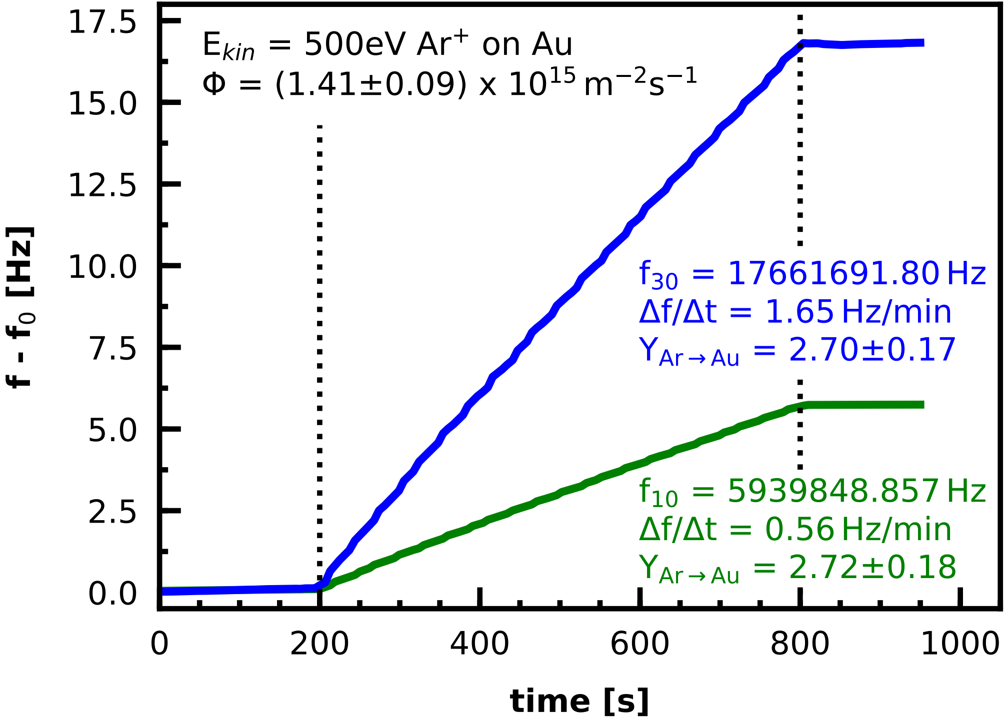
E_{kin} = 500eV Ar^+ on Au
Φ = (1.41±0.09) x $10^{15}\,m^{-2}s^{-1}$
f_{30} = 17661691.80 Hz
$\Delta f/\Delta t$ = 1.65 Hz/min
$Y_{Ar \rightarrow Au}$ = 2.70±0.17
f_{10} = 5939848.857 Hz
$\Delta f/\Delta t$ = 0.56 Hz/min
$Y_{Ar \rightarrow Au}$ = 2.72±0.18
f - f_0 [Hz]
17.5
15.0
12.5
10.0
7.5
5.0
2.5
0.0
0
200
400
600
800
1000
time [s]

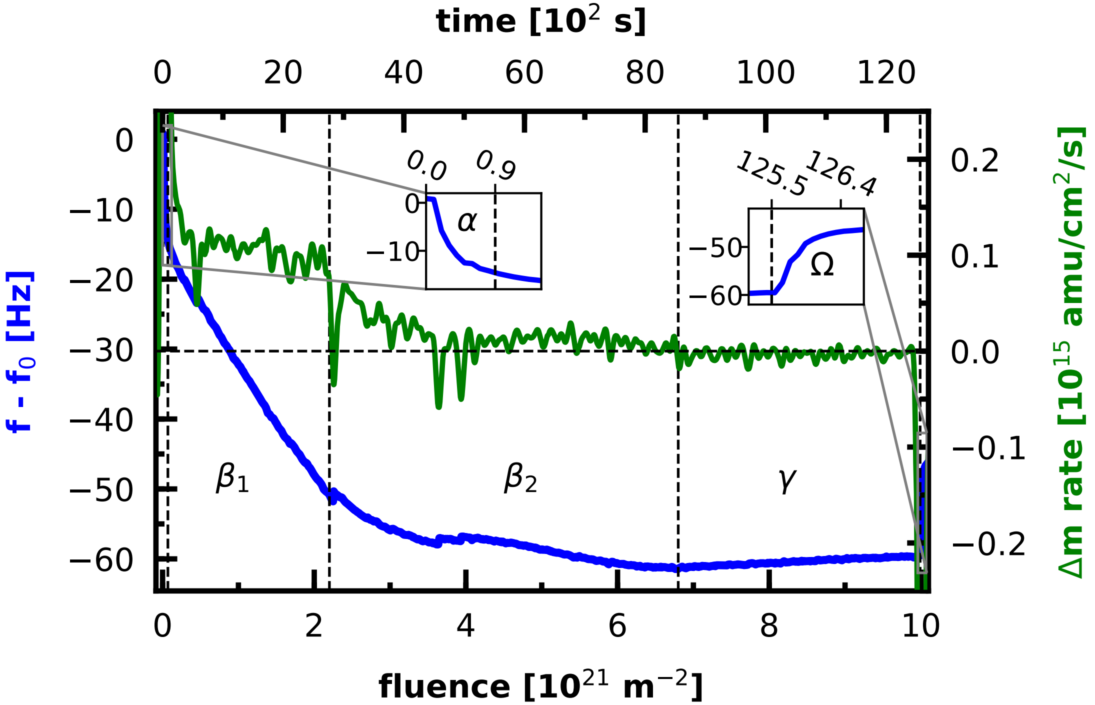
time [10^2 s]
0
20
40
60
80
100
120
f - f$_0$ [Hz]
0
−10
−20
−30
−40
−50
−60
Δm rate [10^{15} amu/cm^2/s]
0.2
0.1
0.0
−0.1
−0.2
0.0
0.9
0
−10
α
125.5
126.4
−50
−60
Ω
β$_1$
β$_2$
γ
0
2
4
6
8
10
fluence [10^{21} m^{-2}]

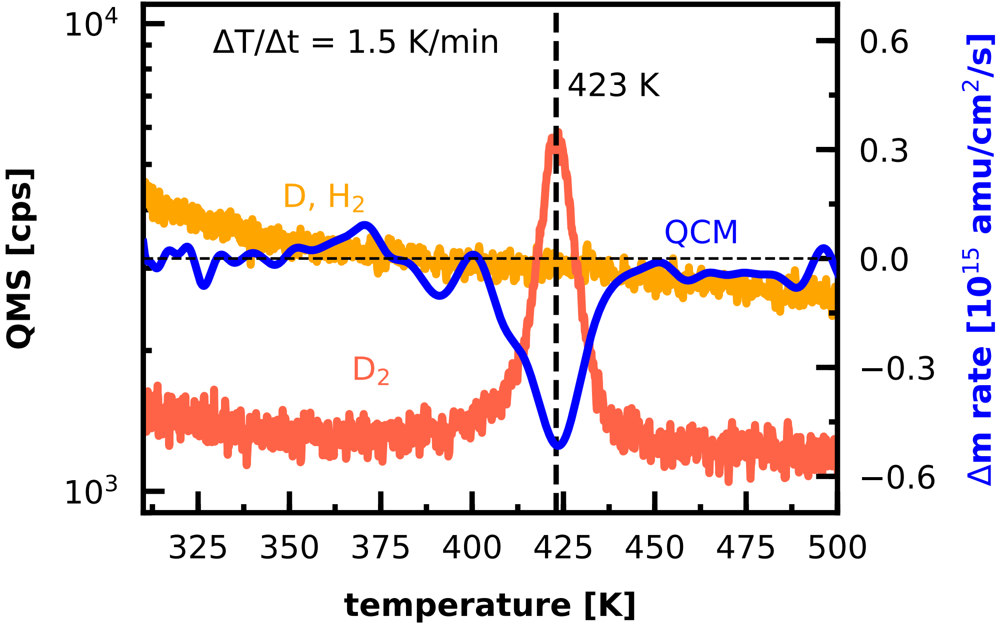
ΔT/Δt = 1.5 K/min
423 K
D, H$_2$
QCM
D$_2$
QMS [cps]
10^4
10^3
0.6
0.3
0.0
−0.3
−0.6
Δm rate [10^{15} amu/cm^2/s]
325
350
375
400
425
450
475
500
temperature [K]